Supplementary Note:

Implementation of Deaths from Comorbidities and Failure Rates

To accurately model progression free survival (PFS) in a lung cancer population for which comorbidities can be significant, a non-cancerous death rate from comorbidities must be considered. Non-cancer related death rates during the 5 yrs. after CRT for lung cancer patients were retrieved from an analysis of the Surveillance, Epidemiology, and End Results (SEER) (1, 2). This analysis stratified the 5 yr. survival probability, death probability from locally-advanced lung cancer, and non-cancerous death probability by age, sex, and severity of comorbidity status. The overall 5 yr. survival probability, cancerous death probability, and non-cancer death probability for the population was calculated to be 15.2%, 71.3%, and 13.5% respectively, given the patient age and sex frequency in the SEER analysis (2) and also the frequency of each comorbidity severity level reported in a separate analysis of SEER data (1). With the current standard of care including PET staging, concurrent chemotherapy, and intensity modulated radiotherapy, the current 5 yr. survival probability from locally-advanced lung cancer was approximated to be 28.8% (averaged 5 yr. overall survival from each arm of the recent PROCLAIM concurrent CRT trial). Assuming the same proportion of deaths from lung cancer and non-cancerous comorbidities but with this same survival probability, the adjusted 5 yr. death probability from cancer and comorbidities was estimated as 59.9% and 11.3%, respectively. The monthly death rate from comorbidities, r_{death}, was then estimated to be 0.55%. The probability of dying from comorbidities on a given discrete month, $t_{month} \in \mathbb{N}$, and the cumulative probability of dying at t_{death} on or before t_{month}, were be then calculated by monthly compounding of r_{death} (**Eqs. S1-S2).** This cumulative distribution function was then inverted and sampled by a drawing a random number, $\zeta \in [0,1]$, to generate a single, stochastic drawing of the time of death by comorbidity $t_{death} \in [0, \infty]$ for each simulated patient **(Eqs. S3-S4**). Finally, the time to progression for an individual patient (**Eq. S7**) was defined as the earliest of time of local failure (LF, **Eq. S5**), time of distant failure (DF, **Eq. S6**), or time of death from comorbidity (t_{death}, **Eq. S4**). Note that LF and DF were assumed to be a multiple of 3 months since the start of treatment, in order to mimic the clinical practice post-treatment evaluation with CT approximately every 3 months.

Death From Comorbidity

pdf $p(t_{month}) = r_{death}(1 - r_{death})^{t_{month}}$ (S1)

cdf $P(t_{death} \leq t_{month}) = 1 - (1 - r_{death})^{t_{month}}$ (S2)

$\zeta = rand \in [0,1]$ (S3)

$t_{death} = \log(-(\zeta - 1))/\log(1 - r_{death})$ (S4)

Tumor Recurrence

$LF = t \leftarrow N_{L_{total}}(t) > N_{L_{total}}[0]$ (S5)

$DF = t \leftarrow N_{D_{total}}(t) > 1cc$ (S6)

$PFS = \min\{LF, DF, t_{death}\}$ (S7)

Hazard Ratio Calculation & Kaplan Meier Analysis

The *lifelines v0.24* package (3) installed in Python 3.7 was used for creating Kaplan Meier (K-M) curves and corresponding 95% confidence intervals. The input to the K-M estimator was a list of time to events (local failure, distant failure or progression) of length N, where N is the

number of simulated patients. For the K-M analysis of the simulated data, patients were assumed to have all started treatment simultaneously with no censorship of patients. Hazard ratios between two population endpoints receiving different treatment schemes were calculated using the Mantel-Haenszel method (4), using the events table of each arm reported by the *lifelines v0.24* package. Statistical significance between two treatments was determined by a log-rank test, calculated by the *lifelines v0.24* python package.

CRT Model Parameter Calibration

The truncated normal and truncated log-normal model parameter distributions published by Geng et al. (5) were used, with the growth and radiosensitivity distributions recalibrated to three single institutional reports of freedom from local and distant failure (FFLF and FFDF) rates in wildtype (WT) and EGFR-mutant locally advanced (LA) NSCLC populations receiving definitive concurrent CRT (6-8). In this analysis, WT specifically refers to a randomly sample from the general population not screened for EGFR status, with reported incidences of EGFR mutations of 24/118 (20%, US) (8), 26/95 (27%, Japan) (7), 29/184 (16%, South Korea) (6) and a mean of 79/397 (20%). The initial stage distribution of the simulated LA-NSCLC population was assumed to be 47% for Stage IIIA and 53% for IIIB as reported in a Phase 3 CRT trial (PROCLAIM) (9). Accordingly, the modeled concurrent CRT treatment was 2 Gy per fraction in 30 fractions of RT (per PROCLAIM) (9) with concurrent chemotherapy (per RTOG 9410 Arm 2) (10) as in our previous work. Optimization was performed where the normalized squared summed difference between the model predicted and the mean literature obtained FFDF or FFLF at 1, 2, 3, and 4 yrs. was calculated over the entire clinically relevant parameter space. For each calibration, five runs with n=1024 simulated patients were performed and aggregated at each parameter value to determine the global optimum (**Suppl. Fig. 1 (A-F)**). The standard deviation of the growth distribution, ρ_σ, and the metastatic fraction, f_{met}, were simultaneously optimized over the FFDF. These parameters were then fixed, and the mean and standard deviation of WT and EGFR-mutant radiosensitivity distributions, α_μ and α_σ, were simultaneously optimized for the WT and EGFR-mutant FFLF, respectively. Confidence intervals (CIs) were estimated via bootstrapping, randomly sampling 512 of the 5120 samples and finding the optimal parameters for 1000 iterations. **Suppl. Fig. 1 (G-I)** shows the 2D joint histogram of the frequency of each of the 1000 optimal model parameters. The 95% confidence interval was then defined by the convex hull (*scipy.spatial.ConvexHull*) that encompasses the closest 95% (i.e. 950) iterations to our global optimum. **Suppl. Fig. 1 (J-L)** shows that the 1000 K-M curves corresponding to the 1000 optimal solutions match the calibration data well and lead to very similar solutions.

For both the model calibration and validation, data was extracted from the literature reported K-M curves with the *WebPlotDigitzer V4.2* program (11). Additionally, the relationship between the model predicted versus literature reported failure rates were quantified with a linear regression, implemented with *linregress* function in the *SciPy* library (12).

TKI Model Parameter Calibration

The TKI model parameters for our simulated population were derived from a previous model based analysis of n=20 tumor volume trajectories in advanced EGFR-mutant NSCLC patients receiving erolitnib (13). Initial persistent fractions of [0.05, 0.2, 0.5] and an initial resistance fractions of [10^{-4}, 10^{-3}, 10^{-2}, 10^{-1}] were modeled in equal proportion, representing a range of

initial TKI sensitivities observed in the patient specific tumor volume trajectories and in an in-vitro clonogenic assay of cells derived from human NSCLC solid tumors (14). Similarly, the TKI cell kill distribution was estimated to be truncated normal with a mean of 2, a standard deviation of 7, and a minimum value of 1, such that the median and maximum TKI cell kill value approximately matched those estimated from the patient specific tumor volume trajectories (patient specific median = 7.8 versus median of truncated normal = $e^{\mu} = e^{2}$ = 7.4; patient specific maximum = 20 versus trunc-norm 99.9th percentile = 21 for n = 1024 simulated patients).

Model Validation Against Clinical Trials

For the model validation against phase 3 clinical trials of CRT alone and TKIs alone, n=1024 patients were simulated having initial persistent fractions of [0.05, 0.2, 0.5] and initial resistance fractions of [10^{-4}, 10^{-3}, 10^{-2}, 10^{-1}] for a total of n=1024x4x3=12288 patients. Histograms of the model parameters are shown in **Suppl. Fig. 4**. The modeled concurrent CRT treatment was implemented the same as in the model calibration per PROCLAIM and per RTOG 9410 Arm 2 while the sequential CRT was implemented per RTOG 9410 Arm 1 with the chemotherapy preceding the radiotherapy (10), resulting in the distant compartment receiving the same treatment in both schedules. Both concurrent chemotherapy arms of the PROCLAIM trial were averaged as no effect was observed. For the model validation against TKIs alone, the TKI treatment was implemented similar to a previous report (13, 15), wherein a daily bolus of erlotinib was administered within a first order pharmacokinetic model resulting in a daily plasma concentration of the drug (**Eq. 14)**. The daily administration continues until progression, as was done in the comparative trials. Additionally, the advanced (stage IV) tumor size distribution from Geng et al. (5) was assumed given the comparative trial was similarly performed in an advanced population. Finally, both the simulated tumor size change from baseline and recurrences were measured every six weeks in accordance with the TKI arm of the EURTAC trial (16).

Multimodal Target-Chemoradiotherapy Treatment Modeling

The two main treatment designs simulated in locally advanced EGFR-mutant NSCLC were TKI induction with daily administration up to 16 weeks, followed by definitive concurrent CRT, followed with or without adjuvant TKI maintenance until a distant or local tumor recurrence. The concurrent CRT was modeled the same as during the model calibration and validation. These two treatment schemes are very similar to ongoing combined TKI+CRT trial protocols: NCT 01822496 -12 wks. TKI induction followed by definitive CRT and NCT 01553942 - 8 wks. TKI induction followed by definitive CRT, followed by surgery if possible, followed by 6 wks. chemotherapy, and finally adjuvant TKI maintenance if there was initial response. Breaks between TKIs and CRT or CRT and TKIs to allow for treatment planning or recovery from symptoms were not explicitly modeled.

Statistical Power Estimation

To analyze the statistical significance of differences in the endpoints between various induction lengths, a Monte Carlo based power calculation was performed to simulate several iterations of a two-arm trial. A short (2 wk.) and a long (12 wk.) induction length arm were simulated with 6 wks. concurrent CRT and adjuvant TKI therapy with n_i = [16, 32, 64,128, 256, 512,1024]

patients in each arm. This was iterated 1000 times by randomizing all N=12288 patients using the *numpy.random.shuffle* routine and again analyzing the first n_i patients (17). For each iteration of each sample size n_i, the median PFS or FFDF of each arm was recorded. The difference in rate of progression or distant failure between the short and long induction lengths was determined to be statistically significant by a log-rank test, which was implemented using the *lifelines v0.24* python package (3). The power as function of sample size was then estimated as the fraction of the 1000 iterations which did reach statistical significance ($p < 0.05$).

Robustness of Results to Pre-existing Resistance and Persistence

The benefit of a shorter induction length was predicted in a generalized population with a spectrum of initial TKI resistant and persistent fractions ($\mathrm{Vr}(0)$ and $\mathrm{Vp}(0)$ respectively). To analyze the robustness of this result to the level of pre-existing resistance and persistence, the short (2 wk.) and long (12 wk.) induction length arms were again simulated with 6 wks. concurrent CRT and adjuvant TKI therapy, for all n=1024 patients of each given combination of $\mathrm{Vr}(0)$ and $\mathrm{Vp}(0)$. Kaplan Meier curves of FFDF and corresponding hazard-ratios were calculated for all 12 combinations $\mathrm{Vr}(0)$ and $\mathrm{Vp}(0)$, shown in **Suppl. Fig. 7.**

Supplementary Data:

Full Parameter Space Analysis of Model Calibration

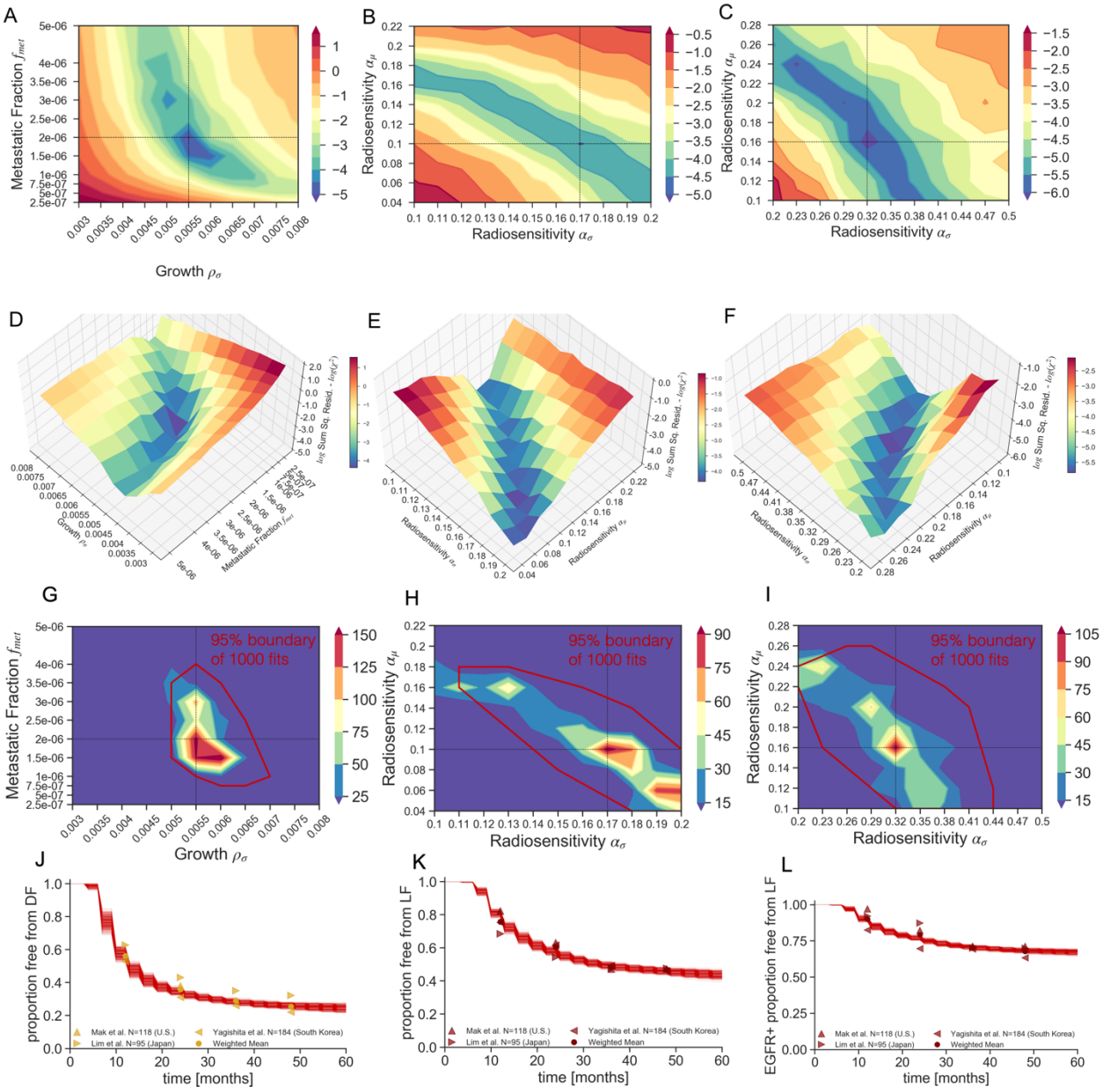

Figure S 1: The model parameter calibration space showing the changes in the $\log_e \chi^2$ residual as a function of initial fraction of metastatic cells and the standard deviation of the growth rate distribution (A, D), the mean and standard deviation of the radiosensitivity distribution for the wildtype (B, E) and EGFR-mutant (C, F) populations. In (A, B, C), the parameter space is shown as a 2D contour map with the optimal parameter values resulting in minimum χ^2 residual denoted with a black dashed line. In (D, E, F) the parameter space is shown as a 3D surface. In (G, H, I), two-dimensional joint histograms of the optimal parameter values for 1000 sub-sampled fits are shown, with the solid red line marking the convex hull in which 95% of the fits closest to the global minimum lie (95% confidence interval). In (J, K, L) K-M curves corresponding to the optimal parameter values for 1000 sub-sampled fits are shown.

Model Simulated PFS for WT and EGFR-mutant Populations Receiving Concurrent Chemoradiotherapy

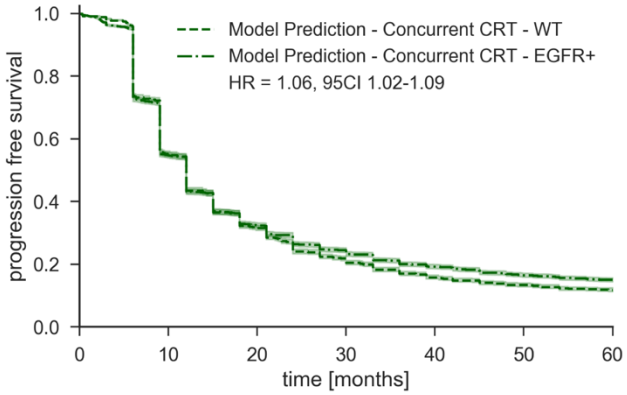

Figure S 2: Simulated progression free survival K-M curves for WT and EGFR-mutant populations with the calibrated model parameters. Even though the radiosensitivity and therefore local control in these two populations differs significantly, the similar distant failure rates lead to similar PFS curves.

Model Predicted Local versus Distant Recurrence Patterns Receiving Sequential Versus Concurrent Chemoradiotherapy

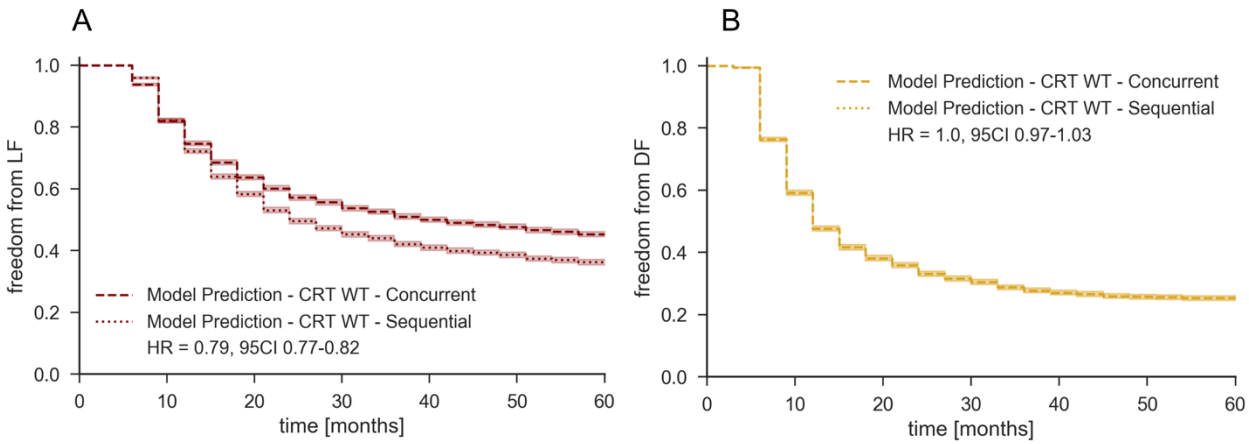

Figure S 3: Model predicted freedom from local failure (A) and distant failure (B) K-M curves for both concurrent and sequential chemoradiotherapy.

Histograms of Model Parameters for Simulated Population

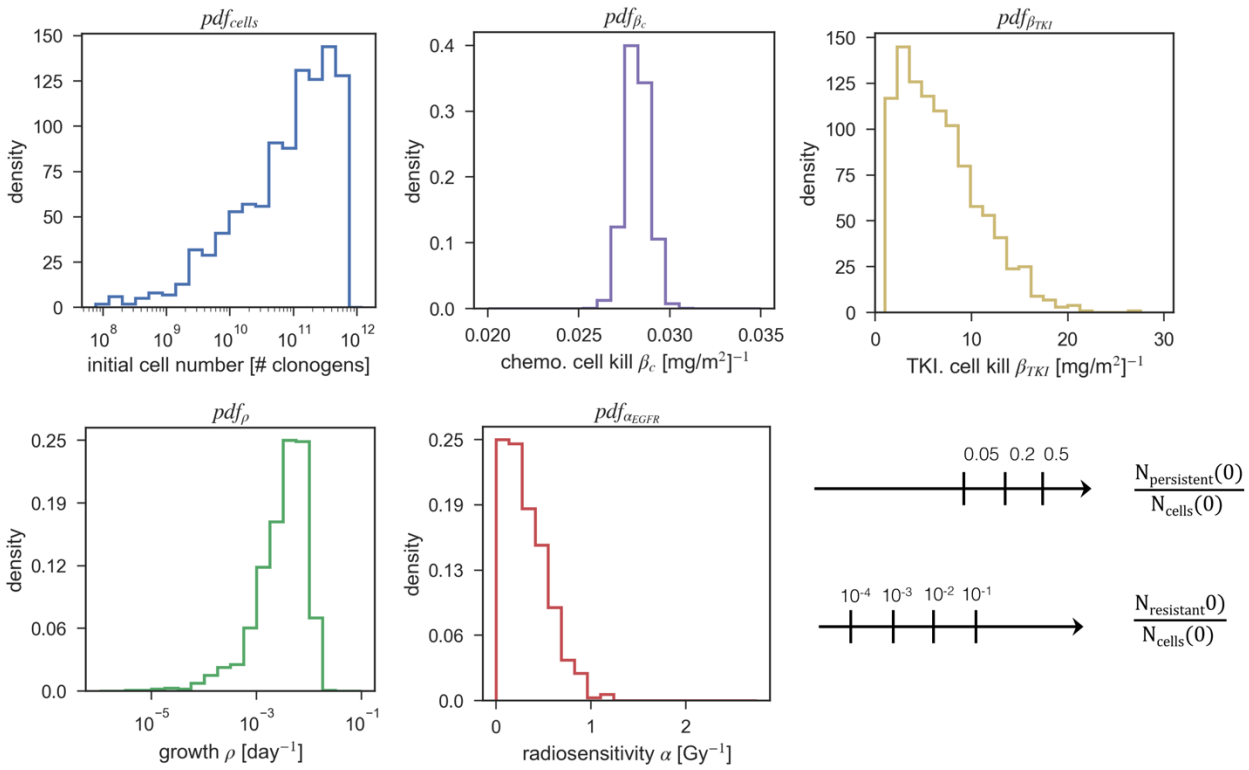

Figure S 4: Distributions of key model parameters used in this work for n=1024 simulated patients with 3 different initial persistent cell fractions and 4 different resistant cell fractions, yielding a total of 3x4x1024 = 12288 simulated patients.

Model Predictions of Full Multimodal Treatment Design Space

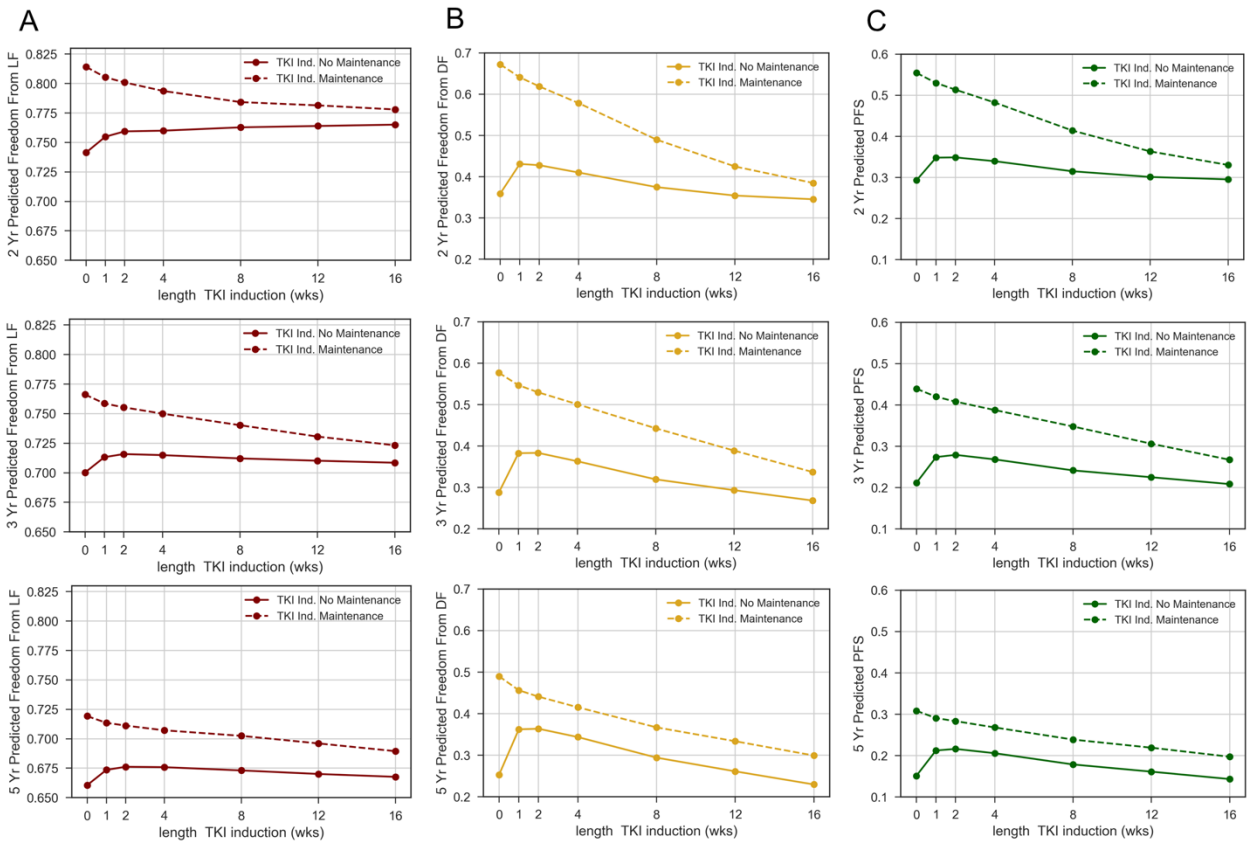

Figure S 5: Plots of FFLF (A), FFDF (B), and PFS (C) as function of induction length both with (solid line) and without (dashed line) adjuvant TKI maintenance at 2 yrs. (top row), 3 yrs. (middle row), and 5 yrs. (bottom row) from start of treatment.

Table of Outcomes for Complete Multimodal Treatment Design Parameter Space

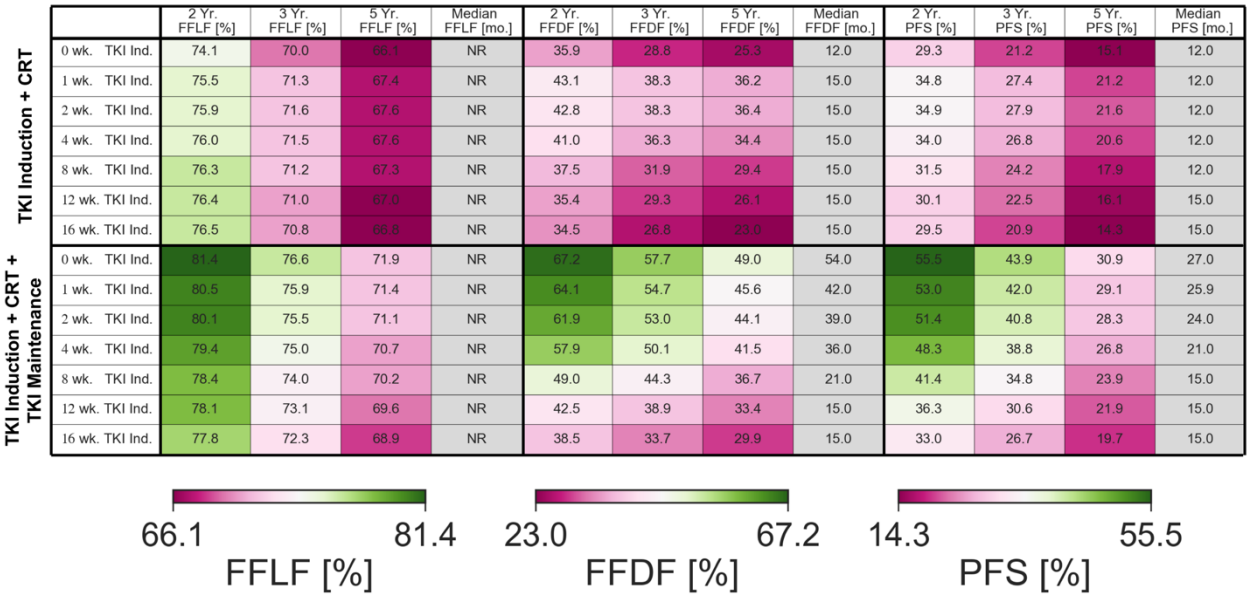

		2 Yr. FFLF [%]	3 Yr. FFLF [%]	5 Yr. FFLF [%]	Median FFLF [mo.]	2 Yr. FFDF [%]	3 Yr. FFDF [%]	5 Yr. FFDF [%]	Median FFDF [mo.]	2 Yr. PFS [%]	3 Yr. PFS [%]	5 Yr. PFS [%]	Median PFS [mo.]
TKI Induction + CRT	0 wk. TKI Ind.	74.1	70.0	66.1	NR	35.9	28.8	25.3	12.0	29.3	21.2	15.1	12.0
	1 wk. TKI Ind.	75.5	71.3	67.4	NR	43.1	38.3	36.2	15.0	34.8	27.4	21.2	12.0
	2 wk. TKI Ind.	75.9	71.6	67.6	NR	42.8	38.3	36.4	15.0	34.9	27.9	21.6	12.0
	4 wk. TKI Ind.	76.0	71.5	67.6	NR	41.0	36.3	34.4	15.0	34.0	26.8	20.6	12.0
	8 wk. TKI Ind.	76.3	71.2	67.3	NR	37.5	31.9	29.4	15.0	31.5	24.2	17.9	12.0
	12 wk. TKI Ind.	76.4	71.0	67.0	NR	35.4	29.3	26.1	15.0	30.1	22.5	16.1	15.0
	16 wk. TKI Ind.	76.5	70.8	66.8	NR	34.5	26.8	23.0	15.0	29.5	20.9	14.3	15.0
TKI Induction + CRT + TKI Maintenance	0 wk. TKI Ind.	81.4	76.6	71.9	NR	67.2	57.7	49.0	54.0	55.5	43.9	30.9	27.0
	1 wk. TKI Ind.	80.5	75.9	71.4	NR	64.1	54.7	45.6	42.0	53.0	42.0	29.1	25.9
	2 wk. TKI Ind.	80.1	75.5	71.1	NR	61.9	53.0	44.1	39.0	51.4	40.8	28.3	24.0
	4 wk. TKI Ind.	79.4	75.0	70.7	NR	57.9	50.1	41.5	36.0	48.3	38.8	26.8	21.0
	8 wk. TKI Ind.	78.4	74.0	70.2	NR	49.0	44.3	36.7	21.0	41.4	34.8	23.9	15.0
	12 wk. TKI Ind.	78.1	73.1	69.6	NR	42.5	38.9	33.4	15.0	36.3	30.6	21.9	15.0
	16 wk. TKI Ind.	77.8	72.3	68.9	NR	38.5	33.7	29.9	15.0	33.0	26.7	19.7	15.0

Figure S 6: Table of outcomes for complete multimodal treatment design parameter space, color coded by range of effect. NR= not reached.

Effect of Pre-existing Resistance and Persistence on Benefit of Shorter Induction

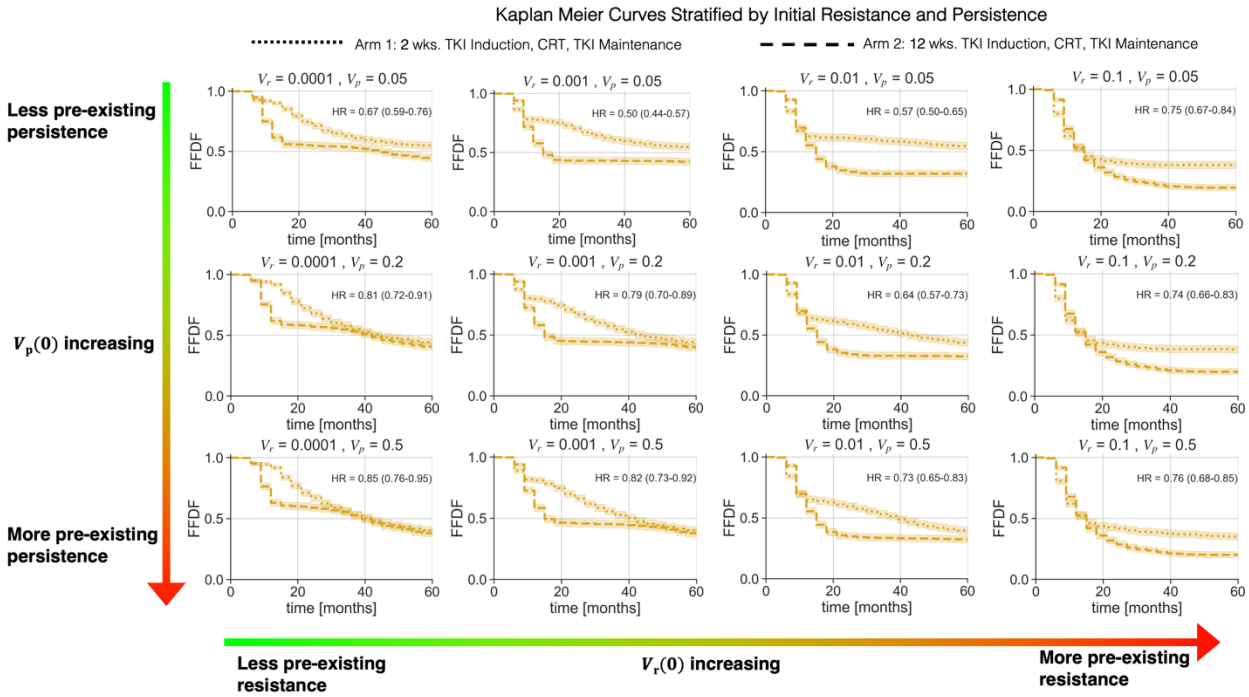

Figure S 7: Simulated *in-silico* induction trial stratified by initial resistance and persistent fractions. Simulated FFDF K-M curves of 2 wk. versus 12 wk. induction lengths for each of the 12 combinations of Vr (Columns) and Vp (Rows). For each Vr, Vp combination the full n=1024 patients were included, and hazard ratios (HR) with 95% confidence intervals are reported. The bounds of all confidence intervals are <1, meaning the benefit of the 2 wk. induction over 12 wk. holds regardless of the initial TKI sensitivity.

Estimated Power of Varying Induction Length on PFS as a Function of Sample Size

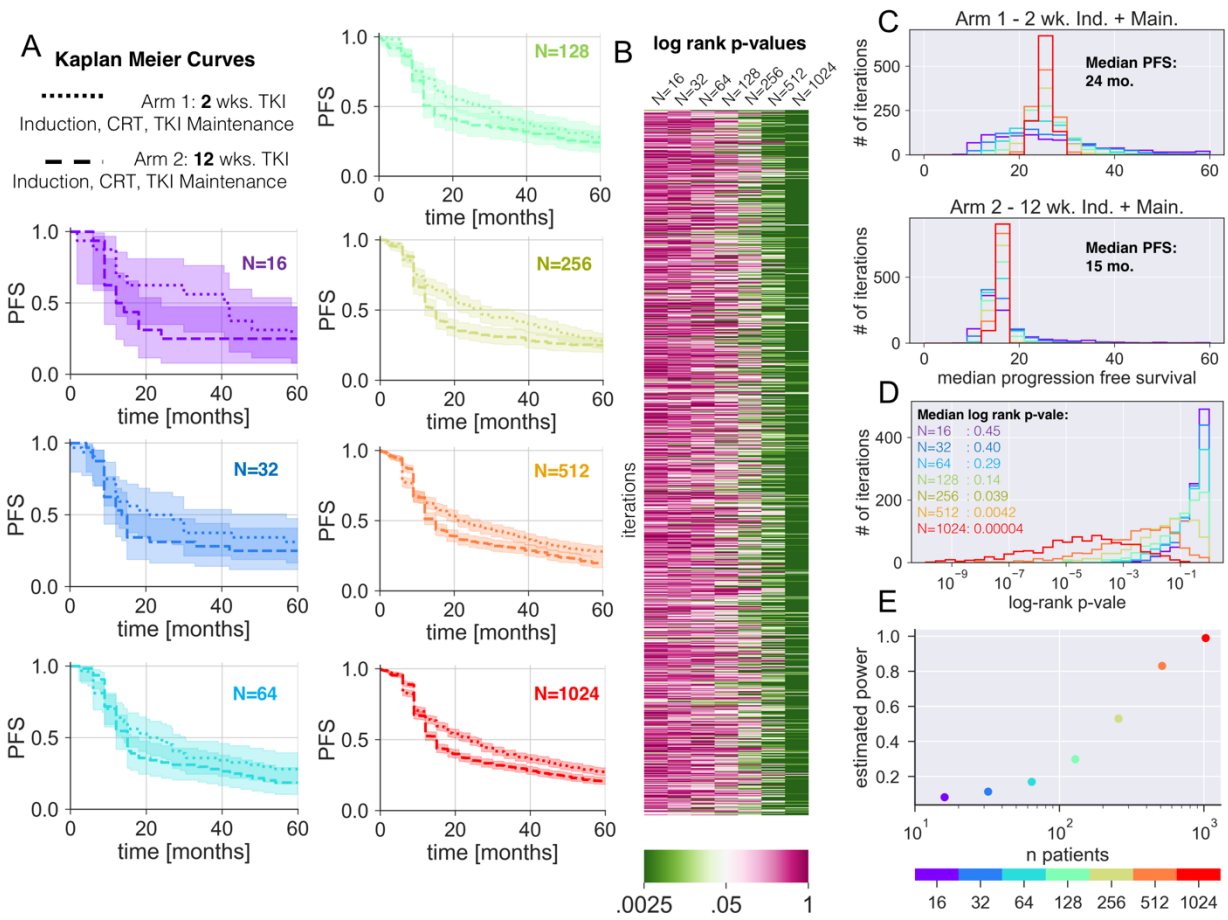

Figure S 8: (A) Simulated PFS K-M curves for 2 wk. and 12 wk. induction lengths with increasing number of simulated patients. (B) A heatmap of log rank p-values testing statistical difference between the 2 wk. versus 12 wk. PFS K-M curves for 1000 iterations of the simulation at each sample size. Histograms of the median PFS (C) and log rank p-values (D) for the 1000 iterations of the 2 wk. and 12 wk. induction simulations at each sample size. Estimated statistical power as a function of sample size. Here statistical was estimated as the fraction of iterations resulting in a p-value<0.05.

Supplementary References:

1. Cho H, Mariotto AB, Mann BS, Klabunde CN, Feuer EJ. Assessing non-cancer-related health status of US cancer patients: other-cause survival and comorbidity prevalence. Am J Epidemiol. 2013;178(3):339-49. doi: 10.1093/aje/kws580. PubMed PMID: 23825168; PMCID: PMC3816346.
2. Edwards BK, Noone AM, Mariotto AB, Simard EP, Boscoe FP, Henley SJ, Jemal A, Cho H, Anderson RN, Kohler BA, Eheman CR, Ward EM. Annual Report to the Nation on the status of cancer, 1975-2010, featuring prevalence of comorbidity and impact on survival among persons with lung, colorectal, breast, or prostate cancer. Cancer. 2014;120(9):1290-314. doi: 10.1002/cncr.28509. PubMed PMID: 24343171; PMCID: PMC3999205.
3. Davidson-Pilon C. CamDavidsonPilon/lifelines: v0.24. v0.24 ed: Zenodo; 2020.
4. Bernstein L, Anderson J, Pike MC. Estimation of the proportional hazard in two-treatment-group clinical trials. Biometrics. 1981;37(3):513-9. PubMed PMID: 7317558.
5. Geng C, Paganetti H, Grassberger C. Prediction of Treatment Response for Combined Chemo- and Radiation Therapy for Non-Small Cell Lung Cancer Patients Using a Bio-Mathematical Model. Sci Rep. 2017;7(1):13542. doi: 10.1038/s41598-017-13646-z. PubMed PMID: 29051600; PMCID: PMC5648928.
6. Lim YJ, Chang JH, Kim HJ, Keam B, Kim TM, Kim DW, Paeng JC, Kang KW, Chung JK, Jeon YK, Chung DH, Wu HG. Superior Treatment Response and In-field Tumor Control in Epidermal Growth Factor Receptor-mutant Genotype of Stage III Nonsquamous Non-Small cell Lung Cancer Undergoing Definitive Concurrent Chemoradiotherapy. Clin Lung Cancer. 2017;18(3):e169-e78. doi: 10.1016/j.cllc.2016.12.013. PubMed PMID: 28131636.
7. Yagishita S, Horinouchi H, Katsui Taniyama T, Nakamichi S, Kitazono S, Mizugaki H, Kanda S, Fujiwara Y, Nokihara H, Yamamoto N, Sumi M, Shiraishi K, Kohno T, Furuta K, Tsuta K, Tamura T. Epidermal growth factor receptor mutation is associated with longer local control after definitive chemoradiotherapy in patients with stage III nonsquamous non-small-cell lung cancer. Int J Radiat Oncol Biol Phys. 2015;91(1):140-8. doi: 10.1016/j.ijrobp.2014.08.344. PubMed PMID: 25442336.
8. Mak RH, Doran E, Muzikansky A, Kang J, Neal JW, Baldini EH, Choi NC, Willers H, Jackman DM, Sequist LV. Outcomes after combined modality therapy for EGFR-mutant and wild-type locally advanced NSCLC. Oncologist. 2011;16(6):886-95. doi: 10.1634/theoncologist.2011-0040. PubMed PMID: 21632451; PMCID: PMC3228219.
9. Senan S, Brade A, Wang LH, Vansteenkiste J, Dakhil S, Biesma B, Martinez Aguillo M, Aerts J, Govindan R, Rubio-Viqueira B, Lewanski C, Gandara D, Choy H, Mok T, Hossain A, Iscoe N, Treat J, Koustenis A, San Antonio B, Chouaki N, Vokes E. PROCLAIM: Randomized Phase III Trial of Pemetrexed-Cisplatin or Etoposide-Cisplatin Plus Thoracic Radiation Therapy Followed by Consolidation Chemotherapy in Locally Advanced Nonsquamous Non-Small-Cell Lung Cancer. J Clin Oncol. 2016;34(9):953-62. doi: 10.1200/JCO.2015.64.8824. PubMed PMID: 26811519.
10. Curran WJ, Jr., Paulus R, Langer CJ, Komaki R, Lee JS, Hauser S, Movsas B, Wasserman T, Rosenthal SA, Gore E, Machtay M, Sause W, Cox JD. Sequential vs. concurrent chemoradiation for stage III non-small cell lung cancer: randomized phase III

trial RTOG 9410. J Natl Cancer Inst. 2011;103(19):1452-60. doi: 10.1093/jnci/djr325. PubMed PMID: 21903745; PMCID: PMC3186782.
11. Rohatgi A. WebPlotDigitizer V4.2. Available from: https://automeris.io/WebPlotDigitizer.
12. Virtanen P, Gommers R, Oliphant TE, Haberland M, Reddy T, Cournapeau D, Burovski E, Peterson P, Weckesser W, Bright J, van der Walt SJ, Brett M, Wilson J, Millman KJ, Mayorov N, Nelson ARJ, Jones E, Kern R, Larson E, Carey CJ, Polat I, Feng Y, Moore EW, VanderPlas J, Laxalde D, Perktold J, Cimrman R, Henriksen I, Quintero EA, Harris CR, Archibald AM, Ribeiro AH, Pedregosa F, van Mulbregt P, SciPy C. SciPy 1.0: fundamental algorithms for scientific computing in Python. Nat Methods. 2020;17(3):261-72. Epub 2020/02/06. doi: 10.1038/s41592-019-0686-2. PubMed PMID: 32015543; PMCID: PMC7056644.
13. Grassberger C, McClatchy DM, Geng C, Kamran SC, Fintelmann F, Maruvka YE, Piotrowska Z, Willers H, Sequist LV, Hata AN, Paganetti H. Patient-specific tumor growth trajectories determine persistent and resistant cancer cell populations during treatment with targeted therapies. Cancer Research. 2019:canres.3652.2018. doi: 10.1158/0008-5472.CAN-18-3652.
14. Hata AN, Niederst MJ, Archibald HL, Gomez-Caraballo M, Siddiqui FM, Mulvey HE, Maruvka YE, Ji F, Bhang HE, Krishnamurthy Radhakrishna V, Siravegna G, Hu H, Raoof S, Lockerman E, Kalsy A, Lee D, Keating CL, Ruddy DA, Damon LJ, Crystal AS, Costa C, Piotrowska Z, Bardelli A, Iafrate AJ, Sadreyev RI, Stegmeier F, Getz G, Sequist LV, Faber AC, Engelman JA. Tumor cells can follow distinct evolutionary paths to become resistant to epidermal growth factor receptor inhibition. Nat Med. 2016;22(3):262-9. doi: 10.1038/nm.4040. PubMed PMID: 26828195; PMCID: PMC4900892.
15. Foo J, Chmielecki J, Pao W, Michor F. Effects of pharmacokinetic processes and varied dosing schedules on the dynamics of acquired resistance to erlotinib in EGFR-mutant lung cancer. J Thorac Oncol. 2012;7(10):1583-93. doi: 10.1097/JTO.0b013e31826146ee. PubMed PMID: 22982659; PMCID: PMC3693219.
16. Rosell R, Carcereny E, Gervais R, Vergnenegre A, Massuti B, Felip E, Palmero R, Garcia-Gomez R, Pallares C, Sanchez JM, Porta R, Cobo M, Garrido P, Longo F, Moran T, Insa A, De Marinis F, Corre R, Bover I, Illiano A, Dansin E, de Castro J, Milella M, Reguart N, Altavilla G, Jimenez U, Provencio M, Moreno MA, Terrasa J, Munoz-Langa J, Valdivia J, Isla D, Domine M, Molinier O, Mazieres J, Baize N, Garcia-Campelo R, Robinet G, Rodriguez-Abreu D, Lopez-Vivanco G, Gebbia V, Ferrera-Delgado L, Bombaron P, Bernabe R, Bearz A, Artal A, Cortesi E, Rolfo C, Sanchez-Ronco M, Drozdowskyj A, Queralt C, de Aguirre I, Ramirez JL, Sanchez JJ, Molina MA, Taron M, Paz-Ares L, Spanish Lung Cancer Group in collaboration with Groupe Francais de P-C, Associazione Italiana Oncologia T. Erlotinib versus standard chemotherapy as first-line treatment for European patients with advanced EGFR mutation-positive non-small-cell lung cancer (EURTAC): a multicentre, open-label, randomised phase 3 trial. Lancet Oncol. 2012;13(3):239-46. doi: 10.1016/S1470-2045(11)70393-X. PubMed PMID: 22285168.
17. Oliphant TE. A guide to NumPy: Trelgol Publishing USA; 2006.